NASA Contractor Report 182030
ICASE Report No. 90–29

ICASE

SPECTRAL SIMULATION OF UNSTEADY COMPRESSIBLE FLOW PAST A CIRCULAR CYLINDER

Wai-Sun Don
David Gottlieb

Contract No. NAS1–18107, NAS1–18605
April 1990

Institute for Computer Applications in Science and Engineering
NASA Langley Research Center
Hampton, Virginia 23665–5225

Operated by the Universities Space Research Association

National Aeronautics and Space Administration
Langley Research Center
Hampton, Virginia 23665-5225

Spectral Simulation of Unsteady Compressible Flow Past a Circular Cylinder

Wai–Sun Don[1]
David Gottlieb[1]

Brown University
Division of Applied Mathematics
Providence, RI 02912

ABSTRACT

An unsteady compressible viscous wake flow past a circular cylinder has been successfully simulated using spectral methods. A new approach in using the Chebyshev collocation method for periodic problems is introduced. We have further proved that the eigenvalues associated with the differentiation matrix are purely imaginary, reflecting the periodicity of the problem. It had been shown that the solution of a model problem has exponential growth in time if "improper" boundary conditions are used. A characteristic boundary condition, which is based on the characteristics of the Euler equations of gas dynamics, has been derived for the spectral code. The primary vortex shedding frequency computed agrees well with the results in the literature for Mach = 0.4 , Re = 80. No secondary frequency is observed in the power spectrum analysis of the pressure data.

[1]Research was supported by the National Aeronautics and Space Administration under NASA Contract Nos. NAS1-18107 and NAS1-18605 while the authors were in residence at the Institute for Computer Applications in Science and Engineering (ICASE), NASA Langley Research Center, Hampton, VA 23665.

1 Introduction

The behavior of the flow past a circular cylinder has been used as the model for fundamental studies of external (open) flows (figure 1.1 shows the schematic of the flow past a circular cylinder). In spite of the simplicity of the geometry, it embodies many interesting features of fluid dynamics, ranging from steady Stokes flow, viscous wake flow to turbulent flow [1]. Morkovin [2] described the behavior of flow past a circular cylinder as the "kaleidoscope of challenging fluid phenomena".

Over the years, the unsteady viscous compressible wake flow past a circular cylinder has been extensively investigated both theoretically and experimentally by many researchers. Theodore von Kàrmàn [3] showed that the formation of the inviscid Karman vortex trail at low Reynolds number (see section 2 for definition) behind a bluff body moving downstream with the flow is linearly stable. The primary vortex shedding frequency is well established both experimentally and numerically over a wide range of Reynolds numbers [4]. If the frequency is nondimensionalized by the free–stream velocity and the diameter of the cylinder, it is called the Strouhal number St in the literature. For example, the Strouhal number of primary vortex shedding frequency St_1 at Reynolds number Re=80 is about 0.156.

A recent paper by Sreenivasan [5] reported experiments indicating that the primary shedding frequency is modulated by a lower secondary frequency, which is not a sub–harmonic to the shedding frequency (see figure 1.2). He suggested that this lower frequency played a major role in the period doubling route to chaos. Moreover, he also observed a discontinuity of the vortex shedding frequency versus Reynolds number (windows of chaos), which was observed earlier by Tritton [6, 7], Berger and Wille [8] and Friehe [9]. Sirovich [10] suggested some possible mechanisms to justify the existence of the secondary frequency. He pointed out that the perturbation and interaction among the vortex pairs can create a secondary frequency. However, Sreenivasan's finding was disputed by Van Atta and Gharib [11], who attributed it to aeroelastic coupling of the flow with the cylinder's vibrating modes.

In light of all these contradictory arguments of the secondary frequency among experimentalists, numerical simulations seem to offer an alternative means of gaining some insight into this controversy. The numerical simulation of unsteady compressible wake flow past a circular cylinder by Townsend, Rudy and Sirovich [12] using a second–order finite–difference scheme seems to confirm the existence of this controversial secondary frequency. The time trace of the pressure and the power spectrum analysis (figure 1.3) clearly shows that the primary shedding frequency was modulated by a lower secondary frequency. The numerical value of the secondary frequency computed, however, is domain size dependent. Karniadakis and Triantafyllou [13] simulated the incompressible flow past a cylinder using the spectral–element technique. No secondary frequency was observed in their simulation. A secondary mode was excited by introducing the forcing term

into the momentum equation.

In this paper we report the results of a collocation (pseudospectral) simulation of the compressible viscous Navier–Stokes equations. Our results demonstrate clearly that the secondary frequency does not exist. However, we had difficulties in imposing outflow boundary conditions in a stable way. In particular the boundary conditions used in [12] yield instabilities in the spectral code. The only set of boundary conditions that stabilized the code will be described in detail and model problems will be analyzed.

When these boundary conditions were implemented in the finite–difference code as well the secondary frequency disappeared. The secondary frequency found in the finite–difference code had been a purely numerical phenomenon. Moreover, Sreenivasan reported that changing the aspect ratio of his wind tunnel, in effect pushing the outer boundaries further away, eliminated the secondary frequency in the experiment.

This research illustrates an important feature of spectral methods. In contrast to the low order (and more robust) finite–difference schemes, spectral methods are less tolerant to incorrect implementation of boundary conditions. Thus the same boundary conditions that produced stable but erroneous results in the finite–difference code were not tolerated in the spectral code. Results with spectral codes are harder to achieve but they are reliable!

This paper is structured as follows: Section 2 describes the governing equations. In section 3 we describe the spectral code based on Chebyshev and Fourier collocation methods. In this section we describe also the filtering used and several options of grid generation. Also in this section we present a proof that the eigenvalues of the Chebyshev method applied to a periodic problem are purely imaginary. Section 4 discusses the boundary conditions, this section is really the heart of this paper. In section 5 we present the numerical results. The conclusion is presented in section 6.

2 Navier–Stokes Equations

The governing equations are the two–dimensional compressible viscous Navier–Stokes equations in strong conservation form [14]. They describe the laws of conservation of mass, momentum and energy in the absence of external forces. This set of equations in the Cartesian coordinates $(x\,,\,y)$ is transformed into the general curvilinear coordinates $(\xi\,,\,\eta)$ with the transformation Jacobian $J = \xi_x\eta_y - \xi_y\eta_x$. The nondimensional form of these equations is

$$\frac{\partial \vec{W}}{\partial t} + \frac{\partial \bar{F}}{\partial \xi} + \frac{\partial \bar{G}}{\partial \eta} = \frac{1}{\mathrm{Re}}\left(\frac{\partial \bar{F}_v}{\partial \xi} + \frac{\partial \bar{G}_v}{\partial \eta}\right) \tag{2.1}$$

where

$$\vec{W} = \frac{1}{J}\begin{bmatrix} \rho \\ \rho u \\ \rho v \\ E \end{bmatrix},$$

$$\begin{aligned} \bar{F} &= \frac{F}{J}\frac{\partial \xi}{\partial x} + \frac{G}{J}\frac{\partial \xi}{\partial y}, \quad \bar{F}_\nu = \frac{F_\nu}{J}\frac{\partial \xi}{\partial x} + \frac{G_\nu}{J}\frac{\partial \xi}{\partial y}; \\ \bar{G} &= \frac{F}{J}\frac{\partial \eta}{\partial x} + \frac{G}{J}\frac{\partial \eta}{\partial y}, \quad \bar{G}_\nu = \frac{F_\nu}{J}\frac{\partial \eta}{\partial x} + \frac{G_\nu}{J}\frac{\partial \eta}{\partial y}; \end{aligned}$$

$$\begin{aligned} F &= \begin{bmatrix} \rho u \\ \rho u^2 + P \\ \rho uv \\ (E+P)u \end{bmatrix}, \quad F_\nu = \begin{bmatrix} 0 \\ \tau_{xx} \\ \tau_{xy} \\ \gamma \kappa \mathrm{Pr}^{-1} \frac{\partial T}{\partial x} + u\tau_{xx} + v\tau_{xy} \end{bmatrix}; \\ G &= \begin{bmatrix} \rho v \\ \rho uv \\ \rho v^2 + P \\ (E+P)v \end{bmatrix}, \quad G_\nu = \begin{bmatrix} 0 \\ \tau_{xy} \\ \tau_{yy} \\ \gamma \kappa \mathrm{Pr}^{-1} \frac{\partial T}{\partial y} + u\tau_{xy} + v\tau_{yy} \end{bmatrix} \end{aligned}$$

coupled with the nondimensional equation of state and the internal energy, respectively,

$$P = (\gamma - 1)\rho T, \quad E = \rho\left[T + \frac{1}{2}(u^2 + v^2)\right].$$

The elements of the stress tensor are

$$\begin{aligned} \tau_{xx} &= \frac{2}{3}\mu\left[2\left(\frac{\partial u}{\partial \xi}\frac{\partial \xi}{\partial x} + \frac{\partial u}{\partial \eta}\frac{\partial \eta}{\partial x}\right) - \left(\frac{\partial v}{\partial \xi}\frac{\partial \xi}{\partial y} + \frac{\partial v}{\partial \eta}\frac{\partial \eta}{\partial y}\right)\right], \\ \tau_{xy} &= \mu\left[\left(\frac{\partial u}{\partial \xi}\frac{\partial \xi}{\partial y} + \frac{\partial u}{\partial \eta}\frac{\partial \eta}{\partial y}\right) + \left(\frac{\partial v}{\partial \xi}\frac{\partial \xi}{\partial x} + \frac{\partial v}{\partial \eta}\frac{\partial \eta}{\partial x}\right)\right], \\ \tau_{yy} &= \frac{2}{3}\mu\left[2\left(\frac{\partial v}{\partial \xi}\frac{\partial \xi}{\partial y} + \frac{\partial v}{\partial \eta}\frac{\partial \eta}{\partial y}\right) - \left(\frac{\partial u}{\partial \xi}\frac{\partial \xi}{\partial x} + \frac{\partial u}{\partial \eta}\frac{\partial \eta}{\partial x}\right)\right] \end{aligned}$$

and

$$\frac{\partial T}{\partial x} = \frac{\partial T}{\partial \xi}\frac{\partial \xi}{\partial x} + \frac{\partial T}{\partial \eta}\frac{\partial \eta}{\partial x}, \quad \frac{\partial T}{\partial y} = \frac{\partial T}{\partial \xi}\frac{\partial \xi}{\partial y} + \frac{\partial T}{\partial \eta}\frac{\partial \eta}{\partial y}.$$

The viscosity is related to the temperature by the Sutherland viscosity law

$$\mu = \frac{c_1 T^{\frac{3}{2}}}{c_2 + T} \tag{2.2}$$

where c_1 and c_2 are constants. The ratio of specific heats γ is 1.4 and the Prandtl number Pr is 0.72. c_v is the specific heat at constant volume and κ is the coefficient of thermal conductivity.

The free–stream Reynolds number $\mathrm{Re} = \rho_\infty U_\infty D/\mu_\infty$ of the flow is based on the diameter of the cylinder D, free–stream velocity U_∞, free–stream density ρ_∞ and dynamic viscosity μ_∞. The

parameter Re in the Navier–Stokes equations (2.1) is the reference Reynolds number computed by the reference quantities $U_{ref} = U_\infty$, $\rho_{ref} = \rho_\infty$, $T_{ref} = U_\infty^2/c_v$. We shall refer to the free–stream Reynolds number as Re unless clarification is deemed necessary.

The Navier–Stokes equations (2.1) and their necessary supplementary relations such as the Sutherland viscosity law (2.2) are characterized by four parameters [14]. These parameters are the free–stream mach number M_∞, free–stream Reynolds number Re, diameter of the cylinder D, and dimensional temperature T_0.

3 The Numerical Method

The 2–D Navier–Stokes equations are solved numerically in polar coordinates with angular (θ) and radial (r) coordinates. Instead of using mapping techniques, such as exponential or algebraic transformations [16, pages 71–75], to map the infinite physical domain into a finite size, the physical domain is simply truncated at some fixed distance away from the cylinder center (see figure 3.1). Typically the outer computational boundary is located about 23 cylinder diameters away from the center of the cylinder.

An O–type grid configuration with branch cut in the center of the wake behind the cylinder is mapped into the computational domain with coordinates $\xi = \xi(\theta)$ and $\eta = \eta(r)$, i.e.,

$$x = r(\eta)\cos\theta(\xi)\,, \quad y = r(\eta)\sin\theta(\xi)\,.$$

The cylinder wall boundary, the outer computational boundary and the periodic–cut boundary are mapped into the four boundaries of the computational domain. This choice of grid structure offers two major numerical advantages. First, the implementation of the boundary conditions is simplified. Secondly, this choice of coordinate system is particularly suited for the employment of the Fourier collocation method in the angular periodic direction and the Chebyshev collocation method in the radial non–periodic direction. They are employed in the form of matrix vector multiplication method instead of the commonly used Fast Fourier Transform method. The reader is referred to [15, 16, 17] et al. for a detailed discussion of these methods.

In some of the numerical experiments, we employed a commonly used exponential filter

$$\sigma_k = \begin{cases} 1 & 0 \le |k| \le k_c \\ e^{-\alpha\left(\frac{k-k_c}{N-k_c}\right)^\gamma} & k_c < |k| \le N \end{cases} \tag{3.1}$$

where k_c is the cut–off frequency, to improve the stability of the spectral scheme. The parameter α is chosen in such a way that it drives σ_N to machine zero ε, i.e., $\alpha = -\ln\varepsilon$. The parameter γ ($\gamma = 4$ or 6 in this research) determines the order of the filter. The filter is incorporated into the solution and differentiation matrices for both the Fourier and Chebyshev collocation methods.

In this application, the important physical phenomena are confined to the viscous wake behind the cylinder and the boundary layer on the cylinder surface. In order to improve the resolution

within these regions without resorting to allocating additional grid points, the grid transformation technique is used for grid point redistribution. Since we found that Chebyshev collocation points provide sufficient resolution within the boundary layer, no additional mapping technique is employed in the radial direction.

The angular grid transformation [18] used is expressed in the complex form

$$e^{i\theta} = \frac{e^{i(\xi-\gamma)} - \beta}{1 - \beta\, e^{i(\xi-\gamma)}} \tag{3.2}$$

where β is a parameter controlling the amount of clustering of grid points at location $\gamma \in [0, 2\pi]$, and $|\beta| < 1$.

The advantages of this grid transformation are summarized as follows :

1. $\theta(\xi)$ and all of its derivatives are analytic and periodic. Hence, the periodic boundary conditions are satisfied and spectral accuracy is retained for spectral methods.
2. $\theta(\xi)$ preserves the periodicity of the Navier–Stokes equations in the angular direction.
3. Analytical transformation derivatives are readily available without resort to numerical approximation, which is usually done in grid generation techniques.

In this numerical simulation of flow past a circular cylinder, $\beta = -0.4$ with $\gamma = 0$ provides a satisfactory resolution within various flow regions in the angular direction. At least half of the grid points used are clustered within the wake region. The other half are distributed around the remaining regions with gradually reduced resolution toward the front of the cylinder (see figure 3.1).

A seemingly attractive alternative to using the Fourier collocation method with mapping is to use the Chebyshev collocation method. As noted before the Chebyshev collocation points are unevenly distributed and cluster at both end points with spacing proportional to $1/N^2$. In our case the two end points coalesce to $\theta = 0$ and this is exactly the region where we need more resolution.

Here we would like to further investigate some aspects of the application of Chebyshev methods for periodic problems. There is more than one way of implementing the above idea. We will discuss one method used for discretization of the first derivative operator and show that it leads to a differentiation matrix with purely imaginary eigenvalues, reflecting the periodicity of the problem.

Consider the model problem

$$u_t = u_x \tag{3.3a}$$

$$u(-1,t) = u(1,t) \tag{3.3b}$$

$$u(x,0) = f(x)\,. \tag{3.3c}$$

The simplest way to apply the Chebyshev collocation (pseudospectral) method to the model problem is to satisfy the equation (3.3a) at the points $\{x_j = \cos(\pi j/N)\ ,\quad j = 1, \ldots, N-1\}$

and to impose the periodicity condition (3.3b). Since the numerical approximation $u_N(x,t)$ is a polynomial of degree N, we need another condition, usually taken to be

$$\frac{\partial u_N}{\partial x}(-1,t) = \frac{\partial u_N}{\partial x}(1,t)\,. \tag{3.4}$$

To summarize u_N satisfies

$$\frac{\partial u_N}{\partial t} = \frac{\partial u_N}{\partial x} + (Ax+B)T_N' \tag{3.5a}$$

$$\begin{aligned} u_N(-1,t) &= u_N(1,t) \\ \tfrac{\partial}{\partial x}u_N(-1,t) &= \tfrac{\partial}{\partial x}u_N(1,t)\,. \end{aligned} \tag{3.5b}$$

For even N, T_N is an even function and T_N' is odd, therefore, $B = 0$ in (3.5a).

We are ready now to state

Theorem 1 *The eigenvalues of the periodic Chebyshev approximation to the first derivative matrix are purely imaginary.*

Proof : Let $\varphi(x,s)$ be an eigenfunction of the first derivative periodic operator and s an eigenvalue then

$$\frac{\partial \varphi}{\partial x} = s\,\varphi - x\,T_N' \tag{3.6a}$$

$$\varphi(-1,s) = \varphi(1,s)\,. \tag{3.6b}$$

Since $\varphi(x,s)$ is a polynomial of degree N in x, it can be written explicitly as

$$\varphi(x,s) = \sum_{k=0}^{\infty} \frac{(x\,T_N')^{(k)}}{s^{k+1}}. \tag{3.7}$$

We denote by

$$\psi(\nu) = \nu\,\varphi(1,\frac{1}{\nu})\,.$$

Thus

$$\begin{aligned} \psi(\nu) &= \sum_{k=0}^{\infty} (x\,T_N')^{(k)}(1)\,\nu^k \\ &= \sum_{k=0}^{\infty} (x\,T_N')^{(2k)}(1)\,\nu^{2k} + \nu \sum_{k=0}^{\infty} (x\,T_N')^{(2k+1)}(1)\,\nu^{2k} \end{aligned}$$

and finally upon setting $\mu = \nu^2$, we get

$$\psi(\nu) = h(\mu) + \nu\,g(\mu) \tag{3.8}$$

where

$$g(\mu) = \sum_{k=0}^{\infty} (x\,T_N')^{(2k+1)}(1)\,\mu^k$$
$$h(\mu) = \sum_{k=0}^{\infty} (x\,T_N')^{(2k)}(1)\,\mu^k$$

It had been shown that the roots of $\psi(\nu)$ have all negative real part, this being a consequence of the stability of the non–periodic Chebyshev method. By the theory of Hurwitz polynomials the roots of $g(\mu)$ and $h(\mu)$ are real and negative.

Substituting (3.7) into (3.6b) we get that the eigenvalues s of the first derivative periodic Chebyshev polynomials satisfy

$$\sum_{k=0}^{\infty} \frac{(x\,T_N')^{(k)}(1) - (x\,T_N')^{(k)}(-1)}{s^k} = 0 \tag{3.9}$$

Now since $x\,T_N'$ is an even polynomial only the even powers of s remain in (3.9). Denoting $\mu = s^{-2}$ (3.9) can be rewritten as $h(\mu) = 0$. The roots μ are real and negative, therefore the eigenvalues s are purely imaginary. This concludes the proof. **Q.E.D.**

A very surprising result follows from a closer look at $h(\mu) = 0$. This equation is the same as the characteristic equation for the Chebyshev second derivative matrix with Dirichlet boundary conditions. Thus the eigenvalues of the first derivative periodic Chebyshev are the square roots of those of the second derivative matrix with Dirichlet boundary conditions.

We plan, in the future, to further investigate the use of the periodic Chebyshev method for the azimuthal direction. In this research we used standard Chebyshev in the radial direction and the mapped Fourier method in the azimuthal direction.

4 Boundary Conditions

In this section, we examine the procedures of imposing various boundary conditions on the outer computational boundary and the cylinder surface. Due to the geometry of this application, the Fourier collocation method enforces the periodicity of all variables automatically in the angular direction. The only challenge is to find a stable procedure in providing boundary conditions at the cylinder surface and the outer computational boundary in the radial direction.

Since, in the present research, the viscous regions are concentrated within the thin boundary layer on the cylinder surface and the narrow near wake behind the cylinder, it is quite reasonable to assume that the flow is basically inviscid at the outer boundary if it is located sufficiently far away from the cylinder. At the cylinder surface, however, viscous flow boundary conditions are used. Also for the present research, the flow is subsonic everywhere. Thus the boundary conditions can be taken from the analysis of hyperbolic equations.

It is well known that great care should be exercised in the application of boundary conditions when spectral methods are used for numerically solving hyperbolic systems of equations. We wish to review here the theory of Chebyshev collocation methods applied to hyperbolic systems. Rather than quote the theorems we wish to illustrate the theory by examples.

Example 1 : Consider the system of equations

$$\begin{aligned} u_t &= u_x + v_x \\ v_t &= \quad - v_x \end{aligned} \tag{4.1}$$

with the boundary conditions

$$u(\pm 1, t) = 0 \tag{4.2}$$

The straightforward application of the Chebyshev method can be summarized in three steps :

A) Given $u(x_j,t), v(x_j,t)$; $x_j = \cos(\pi j/N)$ $j = 0,\ldots,N$ form $\frac{\partial u}{\partial x}(x_j,t)$ and $\frac{\partial v}{\partial x}(x_j,t)$.

B) Use a time marching technique to get $u(x_j, t+\Delta t)$ and $v(x_j, t+\Delta t)$ again for $j = 0,\ldots,N$.

C) Change $u(x_0, t+\Delta t)$ and $u(x_N, t+\Delta t)$ to satisfy the boundary conditions (4.2).

Thus the values of v at the boundaries are taken from step B.

We wish to demonstrate that the procedure outlined above is unstable. Consider the eigenvalue associated with (4.1) :

$$s\hat{u} = \hat{u}_x + \hat{v}_x + (Ax + B)T'_N \tag{4.3a}$$

$$s\hat{v} = \quad -\hat{v}_x \tag{4.3b}$$

$$\hat{u}(\pm 1, s) = 0 \tag{4.3c}$$

where $\hat{u}$ and $\hat{v}$ are Nth degree polynomials in x. Equation (4.3a,b,c) reflects the fact that the boundary conditions are imposed on the variable u only.

Close inspection of (4.3b) reveals that $\hat{v} = 0$. The reason is that the left hand side of (4.3b) is a polynomial of degree N whereas the right hand side is a polynomial of degree $N-1$. Thus we are left with the equation

$$s\hat{u} = \hat{u}_x + \hat{v}_x + (Ax + B)T'_N \tag{4.4a}$$

$$\hat{u}(\pm 1, s) = 0 \tag{4.4b}$$

A polynomial solution of (4.4a) can be expressed in the form

$$\hat{u}(x,s) = A\sum_{k=0}^{\infty} \frac{(x\,T'_N)^{(k)}}{s^{k+1}} + B\sum_{k=0}^{\infty} \frac{(T'_N)^{(k)}}{s^{k+1}}$$

Equation (4.4b) reads now

$$A\sum_{k=0}^{\infty}\frac{(x\,T_N')^{(k)}(1)}{s^{k+1}}+B\sum_{k=0}^{\infty}\frac{(T_N')^{(k)}(1)}{s^{k+1}}\;=0 \tag{4.5a}$$

$$A\sum_{k=0}^{\infty}\frac{(x\,T_N')^{(k)}(-1)}{s^{k+1}}+B\sum_{k=0}^{\infty}\frac{(T_N')^{(k)}(-1)}{s^{k+1}}\;=0 \tag{4.5b}$$

Upon adding and subtracting (4.5a) and (4.5b) and making use of the fact that $x\,T_N'$ is even and T_N' is odd, one gets

$$\begin{aligned} A\sum_{k=0}^{\infty}(x\,T_N')^{(2k)}(1)\,\nu^{(2k)}+B\sum_{k=0}^{\infty}(T_N')^{(2k+1)}(1)\,\nu^{(2k+1)} &= 0\\ A\sum_{k=0}^{\infty}(x\,T_N')^{(2k+1)}(1)\,\nu^{(2k+1)}+B\sum_{k=0}^{\infty}(T_N')^{(2k)}(1)\,\nu^{(2k)} &= 0 \end{aligned} \tag{4.6}$$

where $\nu=1/s$.
We denote by

$$\begin{aligned} g_1(\nu^2) &= \sum_{k=0}^{\infty}(x\,T_N')^{(2k+1)}(1)\,\nu^{(2k)}, \qquad h_1(\nu^2)=\sum_{k=0}^{\infty}(x\,T_N')^{(2k)}(1)\,\nu^{(2k)},\\ g_2(\nu^2) &= \sum_{k=0}^{\infty}(T_N')^{(2k+1)}(1)\,\nu^{(2k)}, \qquad h_2(\nu^2)=\sum_{k=0}^{\infty}(T_N')^{(2k)}(1)\,\nu^{(2k)}. \end{aligned} \tag{4.7}$$

So that (4.6) can be written as

$$\begin{aligned} A\;\; h_1(\nu^2)+B\,\nu\,g_2(\nu^2) &= 0\\ A\,\nu\,g_1(\nu^2)+B\;\; h_2(\nu^2) &= 0 \end{aligned} \tag{4.8}$$

Thus the eigenvalues are determined by the characteristic equation

$$h_1(\nu^2)\,h_2(\nu^2)-\nu^2\,g_1(\nu^2)\,g_2(\nu^2)=0 \tag{4.9}$$

Equation (4.9) is expressed in term of $\nu^2=\mu$. Thus the only possibility for eigenvalues s without positive real part is that the polynomial

$$h_1(\mu)\,h_2(\mu)-\mu\,g_1(\mu)\,g_2(\mu)=0 \tag{4.10}$$

has real negative roots.

Equation (4.10) is a special case of equation (4.10) in [19] with $\alpha=\beta=\gamma=\delta$. The solution in these cases must have positive real part since it approximates a solution of the form e^{t-x}. Thus ν must have positive real part. This conclude the proof.

Example 2 : Consider again equation (4.1)–(4.2). Define

$$w(x,t)=2\,u(x,t)+v(x,t) \tag{4.11}$$

then it is clear that

$$\begin{aligned} \frac{\partial w}{\partial t} &= \frac{\partial w}{\partial x} \\ \frac{\partial v}{\partial t} &= -\frac{\partial v}{\partial x} \end{aligned} \tag{4.12}$$

with the boundary conditions

$$\begin{aligned} w(1,t) &= v(1,t) \\ w(-1,t) &= v(-1,t) \end{aligned} \tag{4.13}$$

The problem (4.12)–(4.13) is identical with (4.1)–(4.2). However the application of the Chebyshev collocation method is different than the one outlined before. Basically the first two steps of the algorithm described above remain unchanged.

In the third step we change not only $u(x,t)$ but also $v(x,t)$ by using equations (4.11)- -(4.12) in the following way :
At $x = -1$ one has to specify $v(-1,t)$ and to use $w(-1,t)$ as computed from steps A) and B). Thus, denoting by $w_c(-1,t+\Delta t)$ the value of $2\,u(-1,t+\Delta t) + v(-1,t+\Delta t)$ we have the system

$$\begin{aligned} 2\,u(-1,t+\Delta t) + v(-1,t+\Delta t) = w(-1,t+\Delta t) &= w_c(-1,t+\Delta t) \\ u(-1,t+\Delta t) &= 0 \end{aligned} \tag{4.14}$$

Equation (4.14) is a system of equations used to update $u(-1,t+\Delta t)$ and $v(-1,t+\Delta t)$. A similar procedure is carried out at the point $x = 1$.

The procedure outlined in (4.14) cast the numerical procedure in the form discussed in [20]. Of course the best procedure is to specify $w(1,t)$ and $v(-1,t)$ and to use $w_c(-1,t)$ and $v_c(1,t)$. This procedure will be used in the current paper and referred to as the *characteristic boundary conditions.*

4.1 Characteristic Boundary Conditions

In this section, we will give the general procedure of how to impose the characteristic boundary conditions at the outer computational boundary followed by the specific implementation for the numerical experiment.

General Procedure

Consider the system of one–dimensional nonlinear hyperbolic partial differential equations with N dependent variables in the conservation form

$$\frac{\partial \vec{W}}{\partial t} + F_x(\vec{W}) = 0 \tag{4.1.1}$$

and the Jacobian of F is defined as $A(\vec{W}) = F_{\vec{w}}$.

The procedure consists of three main steps : *linearization, characteristic decomposition* and *characteristic treatment.*

Linearization :

Equation (4.1.1) is linearized around some uniform state $\vec{w}_0$, i.e.,

$$\frac{\partial \vec{W}}{\partial t} + A(\vec{w}_0)\frac{\partial \vec{W}}{\partial x} = 0 \tag{4.1.2}$$

where the linearized Jacobian $A(\vec{w}_0)$ is a constant $N \times N$ matrix.

Characteristic decomposition :

The system (4.1.2), which is a hyperbolic system with constant coefficients, is diagonalized into the characteristic form, i.e.,

$$\frac{\partial R_i}{\partial t} + \lambda_i \frac{\partial R_i}{\partial x} = 0\,, \quad i = 1,2,\ldots,N \tag{4.1.3}$$

where λ_i are eigenvalues and $R_i = R_i(\vec{W}\,,\,\vec{w}_0)$ are characteristic variables (eigenfunctions).

The sign of each eigenvalue λ_i is then examined at each outer computational boundary point. Suppose that

$$\begin{cases} \lambda_i > 0 & i = 1,\ldots,k \\ \lambda_i < 0 & i = k+1,\ldots,N \end{cases}\,, \tag{4.1.4}$$

then k quantities must be specified and $N-k$ quantities should be obtained numerically at that boundary point.

Characteristic treatment :

Let $\vec{w}_{nu}$ denote the numerical value at the outer computational boundary. Spectral methods update every grid point in the domain, including all of the boundary points, at each time step. No additional extrapolation procedure is needed for the boundary values. Furthermore, we denote $\vec{w}_{al}$ to be the known value of the far–field conditions, for example the free–stream conditions at infinity.

According to the linear theory, the characteristic quantities $R_i(\vec{W}\,,\,\vec{w}_0), i = 1,\ldots,k$ should be specified and the functions $R_i(\vec{W}\,,\,\vec{w}_0), i = k+1,\ldots,N$ should be obtained from the numerical scheme. Thus

$$\begin{aligned} R_i(\vec{W}\,,\,\vec{w}_0) &= R_i(\vec{w}_{al}\,,\,\vec{w}_0)\,, \quad i = 1,\ldots,k \\ R_i(\vec{W}\,,\,\vec{w}_0) &= R_i(\vec{w}_{nu}\,,\,\vec{w}_0)\,, \quad i = k+1,\ldots,N\,. \end{aligned} \tag{4.1.5}$$

This process results in a linear system of N equations with N unknowns. Once solved, this system of equations yields $\vec{W}$ at each boundary point. We will henceforth denote this procedure as *characteristic boundary conditions.*

Characteristic Boundary Conditions for the 2–D Euler Equations of Gas Dynamics

Following the general procedure outlined in the previous section, we will derive the characteristic boundary conditions for the 2–D Euler equations of gas dynamics.
Let us denote

$$\begin{aligned}
\vec{U}_\infty &= (u_\infty, v_\infty) = (1, 0) && \text{to be the free–stream velocity,} \\
\vec{M} &= (m_u, m_v) = (\rho u, \rho v) && \text{to be the mass flux,} \\
c &= \sqrt{\gamma(\gamma-1)T_\infty} && \text{to be the local free–stream sound speed,} \\
\vec{N} &= \left(\frac{\widetilde{\partial \eta}}{\partial x}, \frac{\widetilde{\partial \eta}}{\partial y}\right) \\
&= (\eta_x, \eta_y)/\sqrt{\eta_x^2 + \eta_y^2} && \text{to be the unit radial normal vector,}
\end{aligned}$$

and $(\rho,\ m_u,\ m_v,\ E)$ to be conserved mass, momentums and internal energy. The subscript ∞ denotes free–stream values.

Linearization :

Consider the 2–D Navier–Stokes equations (2.1),

$$\frac{\partial \vec{W}}{\partial t} + \frac{\partial \bar{F}}{\partial \xi} + \frac{\partial \bar{G}}{\partial \eta} = \frac{1}{\mathrm{Re}}\left(\frac{\partial \bar{F}_\nu}{\partial \xi} + \frac{\partial \bar{G}_\nu}{\partial \eta}\right)$$

where $\vec{W} = (\rho,\ m_u,\ m_v,\ E)^t$.

Far away from the boundary layer on the cylinder surface, the flow is dominated by the convective term and viscosity exerts only a minor effect except inside the narrow wake. Hence, by assuming ν is small or Re is large, (2.1) becomes the 2–D nonlinear Euler equations in strong conservation form. The nonlinear Euler equations can then be linearized with the free–stream conditions $\vec{w}_0 = (\rho_\infty, \vec{M}_\infty, E_\infty)$, i.e.,

$$\frac{\partial \vec{W}}{\partial t} + A_\infty \frac{\partial \vec{W}}{\partial r} + B_\infty \frac{\partial \vec{W}}{\partial \theta} = 0 \qquad (4.1.6)$$

where A_∞ and B_∞ are constant Jacobian matrices in the radial and angular directions respectively. Since we are only interested in deriving the boundary conditions in the radial direction, we can drop the angular dependent term $B_\infty \frac{\partial}{\partial \theta}\vec{W}$ from consideration.

Characteristic decomposition :

It is a matter of algebra to find the eigenvalues λ_i and their corresponding characteristic variables R_i of A_∞. They are

$$\lambda_1 = \lambda_2 = \vec{U}_\infty \cdot \vec{N}\ , \quad \lambda_3 = \vec{U}_\infty \cdot \vec{N} - c\ , \quad \lambda_4 = \vec{U}_\infty \cdot \vec{N} + c\ , \qquad (4.1.7)$$

and

$$
\begin{aligned}
R_1 &= \rho\frac{c^2}{\gamma-1} - \left(\frac{1}{2}\rho\vec{U}_\infty\cdot\vec{U}_\infty - \vec{M}\cdot\vec{U}_\infty + E\right) \\
R_2 &= (m_u - \rho\, u_\infty)\widetilde{\frac{\partial\eta}{\partial y}} - (m_v - \rho\, v_\infty)\widetilde{\frac{\partial\eta}{\partial x}} \\
R_3 &= -(\vec{M} - \rho\vec{U}_\infty)\cdot\vec{N} + \left(\frac{\gamma-1}{c}\right)\left(\frac{1}{2}\rho\vec{U}_\infty\cdot\vec{U}_\infty - \vec{M}\cdot\vec{U}_\infty + E\right) \\
R_4 &= (\vec{M} - \rho\vec{U}_\infty)\cdot\vec{N} + \left(\frac{\gamma-1}{c}\right)\left(\frac{1}{2}\rho\vec{U}_\infty\cdot\vec{U}_\infty - \vec{M}\cdot\vec{U}_\infty + E\right).
\end{aligned}
\tag{4.1.8}
$$

Characteristic boundary conditions :

The values of all conservative variables are assumed to be known at the outer computational boundary.

At the subsonic inflow region, i.e., $\vec{U}_\infty\cdot\vec{N} < 0$ and $\vec{U}_\infty\cdot\vec{N} < c$, one gets

$$\lambda_i < 0\,, \quad i = 1,2,3 \qquad ; \qquad \lambda_4 > 0$$

from (4.1.7). Accordingly,

$$
\begin{aligned}
R_i(\rho\,,\vec{M}\,,E) &= F_i \stackrel{\text{def}}{=} R_i(\rho_\infty\,,\vec{M}_\infty\,,E_\infty)\,, \quad i = 1,2,3 \\
R_4(\rho\,,\vec{M}\,,E) &= F_4 \stackrel{\text{def}}{=} R_4(\rho_{nu}\,,\vec{M}_{nu}\,,E_{nu})
\end{aligned}
\tag{4.1.9}
$$

should be used at each inflow boundary point.

At the subsonic outflow region, i.e., $\vec{U}_\infty\cdot\vec{N} > 0$ and $\vec{U}_\infty\cdot\vec{N} < c$, one gets

$$\lambda_i > 0\,, \quad i = 1,2,4 \qquad ; \qquad \lambda_3 < 0$$

from (4.1.7) instead. Accordingly,

$$
\begin{aligned}
R_i(\rho\,,\vec{M}\,,E) &= F_i \stackrel{\text{def}}{=} R_i(\rho_{nu}\,,\vec{M}_{nu}\,,E_{nu})\,, \quad i = 1,2,4 \\
R_3(\rho\,,\vec{M}\,,E) &= F_3 \stackrel{\text{def}}{=} R_3(\rho_\infty\,,\vec{M}_\infty\,,E_\infty)
\end{aligned}
\tag{4.1.10}
$$

should be used at each outflow boundary point.

Remark : Since the grid structure can be constructed in such a way that $\vec{N} \neq (0\,,1)$ at any outer boundary point, the case of $\vec{U}_\infty\cdot\vec{N} = 0$ will never arise in this application.

More specifically, equations (4.1.8), (4.1.9) and (4.1.10) together yield

$$F_1 = \rho\frac{c^2}{\gamma-1} - \left(\frac{1}{2}\rho\vec{U}_\infty\cdot\vec{U}_\infty - \vec{M}\cdot\vec{U}_\infty + E\right)$$

$$
\begin{aligned}
F_2 &= (m_u - \rho\, u_\infty)\,\widetilde{\frac{\partial \eta}{\partial y}} - (m_v - \rho\, v_\infty)\,\widetilde{\frac{\partial \eta}{\partial x}} \\
F_3 &= -(\vec{M} - \rho\,\vec{U}_\infty)\cdot\vec{N} + \left(\frac{\gamma-1}{c}\right)\left(\frac{1}{2}\rho\,\vec{U}_\infty\cdot\vec{U}_\infty - \vec{M}\cdot\vec{U}_\infty + E\right) \\
F_4 &= (\vec{M} - \rho\,\vec{U}_\infty)\cdot\vec{N} + \left(\frac{\gamma-1}{c}\right)\left(\frac{1}{2}\rho\,\vec{U}_\infty\cdot\vec{U}_\infty - \vec{M}\cdot\vec{U}_\infty + E\right).
\end{aligned}
\tag{4.1.11}
$$

It is easy to check that if

$$
\phi_1 = \frac{c}{\gamma-1}\frac{(F_3+F_4)}{2}\,, \quad \phi_2 = \frac{1}{2}(F_4 - F_3)\,, \quad \phi_3 = F_2 \quad ,
$$

then the solution of (4.1.11) is

$$
\begin{aligned}
\rho &= \frac{\gamma-1}{c^2}(F_1 + \phi_1) \\
m_u &= (\phi_2\,\widetilde{\eta_x} + \phi_3\,\widetilde{\eta_y}) + \rho\, u_\infty \\
m_v &= (\phi_2\,\widetilde{\eta_y} - \phi_3\,\widetilde{\eta_x}) + \rho\, v_\infty \\
E &= \phi_1 - \frac{1}{2}\rho\,\vec{U}_\infty\cdot\vec{U}_\infty + m_u u_\infty + m_v v_\infty\,.
\end{aligned}
\tag{4.1.12}
$$

The primitive variables (ρ, u, v, T) can then be extracted from (4.1.12) at each outer computational boundary point.

4.2 Cylinder Surface Boundary Conditions

At the cylinder surface, the no–slip and constant temperature boundary conditions are enforced, i.e.,

$$
u = v = 0\,, \quad T = T_\infty\,, \quad \rho = \rho_{cal}\,, \tag{4.2.1}
$$

where ρ_{cal} is the density computed numerically by the spectral code.

5 Numerical Results and Discussion

The spectral code is fully vectorized to take advantage of the vector pipeline hardware architecture of the Cyber 205 supercomputer at the NASA Langley Research Center. Based on the free–stream flow conditions ($U_\infty = 186.0\,\mathrm{m/sec}$, $T_\infty = 538.3\,K$, $P_\infty = 30.61\,\mathrm{Pa}$) and the cylinder diameter $D = 61.0\,\mathrm{mm}$, all the computations are made at free–stream Mach number, Mach $= 0.4$, and free–stream Reynolds number, Re $= 80$.

To advance the flow field in time, the second–order Runge–Kunta method is employed. The initial flow is started impulsively (uniform free–stream conditions throughout the whole domain except the no–slip and constant temperature boundary conditions at the cylinder surface). After the transient effect of the initial conditions has diminished from the flow–field, the numerical

scheme is integrated over 20,000 or more time steps providing enough cycles of vortex shedding for analysis. The time trace of the pressure signal at several locations is recorded and stored for later power density spectrum analysis using the Discrete Fast Fourier Transform (DFFT) technique. The chosen point for which the signal was analyzed is located at approximately $1D$ above the wake centerline and $10D$ behind the cylinder within the wake (X_{wk}). We also recorded the pressure signal at location $10D$ away from the cylinder center and 180 degrees around the cylinder in the inflow region (X_{in}). In order to be able to compare the numerical results with the experimental results, the signal point X_{wk} is located approximately at the position of the hot wire probe in some experiments of Sreenivasan.

Each set of time series contains the nondimensionalized pressure $P(t)/P_\infty$ at each time step. Since we are only interested in the perturbation signal superimposed on the uniform flow, the average of $P(t)/P_\infty$ is first subtracted from each data set. The resulting time series $\hat{P}(t)$ is analyzed in the frequency domain in order to identify individual dominant frequencies. This is usually accomplished by the power density spectrum analysis. A discrete time series $\hat{P}(t_n)$ of length T is transformed into the frequency space by the Discrete Fast Fourier Transform technique.

If f, k and Δt denote the frequency, the wave number and the time increment respectively, then

$$\hat{P}(t_n) = \sum_{k=-N}^{k=N} a_k e^{i2\pi \frac{kn}{N}}$$

where $T = N\Delta t$, $t_n = n\Delta t$ and $k = fT$.

For each wave number k, the complex coefficient a_k is multiplied by its conjugate $\bar{a}_k$, i.e. $b_k = a_k \bar{a}_k$. $\{ b_k, \ k = 0, \ldots, N \}$ is called the power spectrum, which measures the energy of each wave number (frequency). Normally, the power of each wave number is plotted using a logarithmic scale of base 10. Those dominant frequency components will show up as sharp peaks in the plotted power spectrum. Since the DFFT of the pressure signal requires a uniform time increment Δt, it is fixed at 0.00434201 after the flow is settled in a regular pattern of alternate vortex shedding.

Spectral Scheme with characteristic boundary conditions – SP1

The resolution of the spectral code, which used 64 × 48 grid points in the angular and radial directions respectively, is comparable to, if not better than, the resolution of the full finite–difference code [12], which used 120×151 gird points. The spectral scheme becomes unstable when the number of grid points used is reduced in either directions. It appears that 64 × 48 is a lower limit of the number of grid points required to achieve the resolution. This conforms to the typical exponential convergence behavior of spectral methods. This should come as no surprise because the spectral code is developed within the theoretical scope of spectral methods. Furthermore, since a lesser number of grid points is employed in the spectral scheme, the larger spacing also allows a larger

time step to be taken in the numerical simulation. Typically, the time step of the spectral code is about 10 times larger than the full finite–difference method.

Figures 5.1a–b show contour plots of density ρ/ρ_∞ and temperature T/T_∞, respectively. The vortices pass through the outer computational boundary without any apparent reflection back into the interior domain. Furthermore, no observable spurious perturbation travels back into the interior domain either. The Karman vortex street is clearly demonstrated in the contour plots.

The pressure time series and its power spectrum at X_{wk} and X_{in} are shown in figures 5.2a–b respectively. As indicated in all the power density spectra, no secondary frequency can be observed both within the wake and in front of the cylinder at the inflow region. The frequencies that appear in the power spectrum are the primary vortex shedding frequency $St_1 = 0.1574$ and its harmonics only.

Spectral Scheme with non–characteristic boundary conditions – SP2

To show the sensitivity of the boundary conditions for spectral methods, we replace the characteristic boundary conditions by the non–characteristic one used in [12]. The initial flow is restarted from the flow–field data of the previous run SP1. The simulation becomes explosively unstable after only 71 time steps.

Scheme	Domain size (D)	Number of time steps	Total time	St_1	St_2
SP1	46 D	20480	88.92	0.1574	none
SP2	46 D	71	unstable		
SP1	41 D	19456	70.26	0.1565	none

Table 1: Results of the spectral simulation of unsteady compressible flow past a circular cylinder with $N_\theta = 64$, $N_r = 48$, Mach = 0.4, Re = 80.

6 Conclusion

An unsteady compressible viscous wake flow past a circular cylinder has been successfully simulated using the Fourier and Chebyshev collocation methods. A new approach in using the Chebyshev collocation method for periodic problems is introduced. We have further proved that the eigenvalues associated with the differentiation matrix are purely imaginary, reflecting the periodicity of the problem. It had been shown that the solution of a model problem has exponential growth in time if "improper" boundary conditions procedure is used. Hence, we derived the characteristic boundary conditions, which is based on the characteristics of the Euler equations of gas dynamics, for the spectral simulation. The primary vortex shedding frequency agrees well with the results in the literature for Mach number 0.4 and Reynolds number 80. No secondary frequency is observed

in the power spectrum analysis of the pressure data that is generated by the spectral code with the characteristic boundary conditions.

Acknowledgement

The research reported here is part of the first author's thesis supported by NASA Langley's Graduate Program in Aeronautics (grant NAG–1–703). The second author was supported in part by the U.S. Air Force of Scientific Research under grant AF–85–0303 and by NSF grant DMS–8810150.

References

[1] G. K. Batchelor, *An Introduction to Fluid Dynamics*, Cambridge University Press (1967)

[2] M. V, Morkovin, *Flow around circular cylinder. A kaleidoscope of challenging fluid phenomena*, Symp. Fully Separated Flows, ed. by G. Hansen, ASME, New York, pp. 102–118 (1974)

[3] T. von Karman, *Uber den Mechanismus des Widerstands, den ein Bewegter Korper in einer Flussigkeit Erfahrt*, Gottiger Nachrichten, Math. Phys. K1., pp. 509–519 (1911)

[4] A. Roshko, *On the development of turbulent wakes from vortex streets*, NACA TN–2913 (1953)

[5] K. R. Sreenivasan, *Transitional and Turbulent Wakes and Chaotic Dynamical Systems*, Frontiers in Fluid Mechanics, ed. by S. H. Davis and J. L. Lumley (Springer, New York, 1985), pp. 41–67

[6] D. J. Tritton, *Experiments on the flow past a circular cylinder at low Reynolds numbers*, J. Fluid Mech. **6**, pp. 547 (1959)

[7] D. J. Tritton, *A note on vortex street behind circular cylinders at low Reynolds number*, J. Fluid Mech. **45**, pp. 203 (1971)

[8] E. Berger, R. Wille, *Periodic flow phenomena*, Ann. Rev. Fluid Mech. **4**, pp. 313 (1972)

[9] C. A. Friehe, *Vortex shedding from cylinders at low Reynolds numbers*, J. Fluid Mech. **100**, pp. 237 (1980)

[10] L. Sirovich, *The Karman vortex trail and flow behind a circular cylinder*, Phys. Fluids **28**, pp. 2723 (1985)

[11] C. W. Van Atta, M. Gharib, *Ordered and Chaotic Vortex Streets Behind Circular Cylinders at Low Reynolds numbers*, J. Fluid Mech. **174**, pp. 113–133 (1987)

[12] J. Townsend, D. Rudy, L. Sirovich, *Computation and Analysis of a Cylinder Wake Flow*, Forum on Unsteady Flow Separation **52**, ASME, pp. 165–174 (1987)

[13] G. E. Karniadakis, G. S. Triantafyllou, *Frequency selection and asymptotic states in laminar wakes*, to be appear in J. Fluid Mech. (1988)

[14] P. J. Roache, *Computational Fluid Dynamics*, Hermosa Publishers, pp. 209–223 (1976)

[15] D. Gottlieb, S. A. Orszag, *Numerical Analysis of Spectral Methods: Theory and Applications*, CBMS conference Series in Applied Mathematics **26**, SIAM, (1977)

[16] C. Canuto, M. Y. Hussaini, A. Quarteroni, T. A. Zang, *Spectral methods in fluid dynamics*, Springer–Verlag (1987)

[17] R. G. Voigt, D. Gottlieb, M.Y. Hussaini (eds.), *Spectral Methods for Partial Differential Equations*, SIAM–CBMS Philadelphia (1984)

[18] J. Augenbaum, *An adaptive pseudospectral method for discontinuous problems*, ICASE report no. 88–54, to appear in Appl. Num. Math. (1988)

[19] D. Gottlieb, L. Lustman, *The Spectrum of the Chebyshev Collocation Operator for the Heat Equation*, SIAM J. Numer. Anal. **20**, pp909–921 (1983)

[20] D. Gottlieb, L. Lustman, C. S. Streett, *Spectral Methods for Two Dimensional Shocks*, in *Spectral Methods for Partial Differential Equations*, ed. by R. G. Voigt, D. Gottlieb, M. Y. Hussaini, (SIAM–CBMS, Philadelphia) pp. 79–95 (1984)

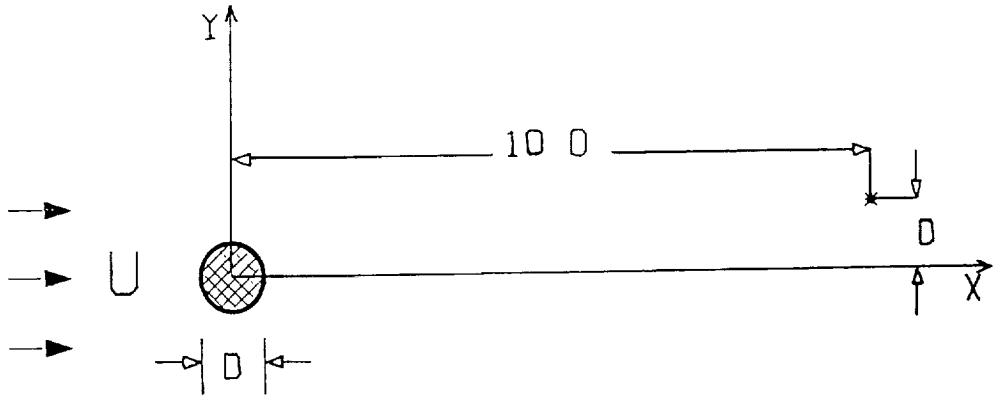

Figure 1.1: Schematic of flow past a circular cylinder of diameter D. The location of the hot wire measurement in Sreenivasan's experiments is marked as * .

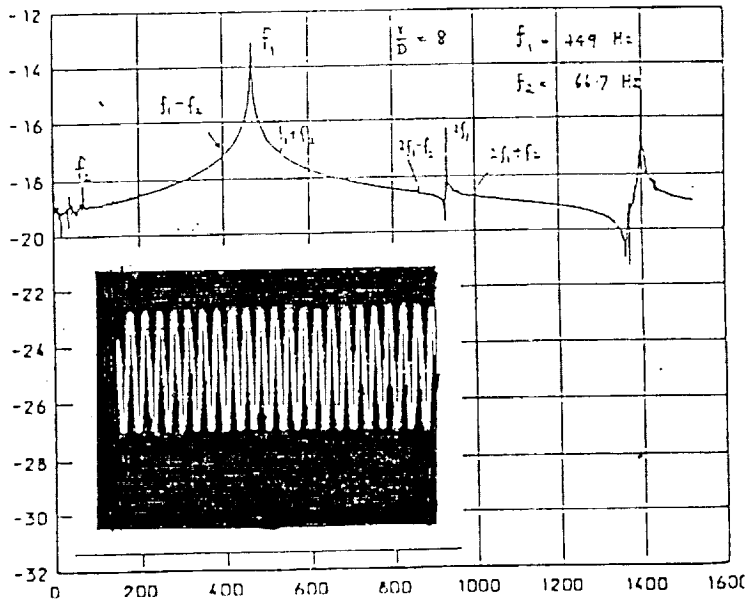

Figure 1.2: The power density spectrum of velocity u at Re=120, $x/D = 8$ as reported by Sreenivasan [5]. The inset shows a typical hot wire aerometer oscillograph. The power is plotted on a logarithmic scale of base 10.

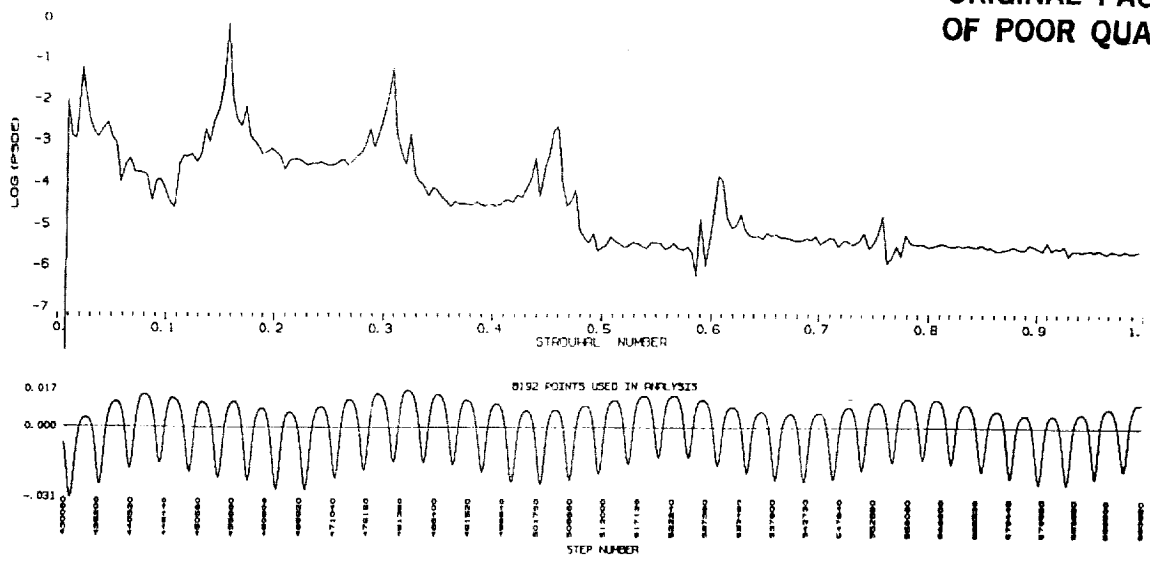

Figure 1.3: The pressure time series and the power density spectrum of the full finite-difference scheme [12].

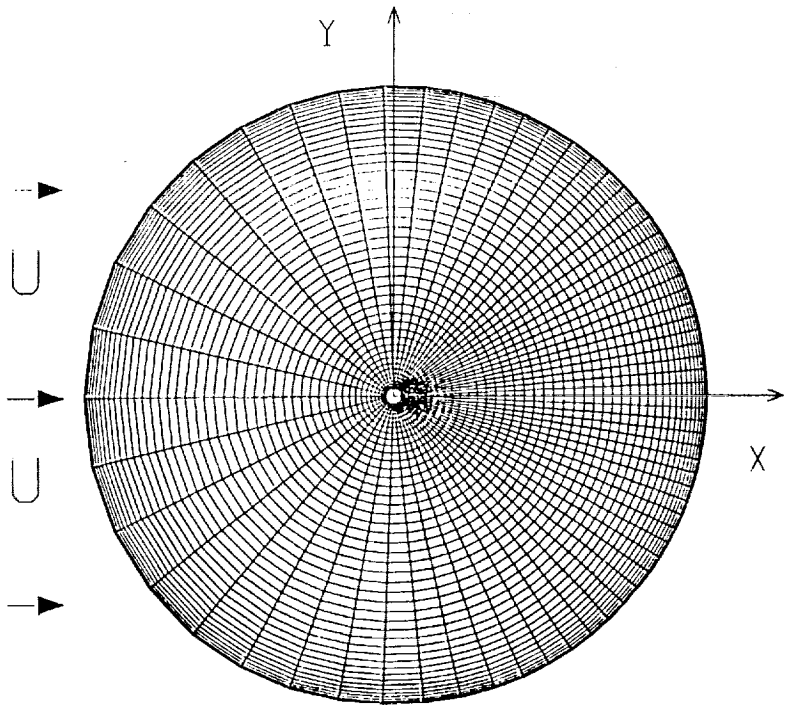

Figure 3.1: The grid structure of flow past a circular cylinder in Cartesian coordinates (x, y).

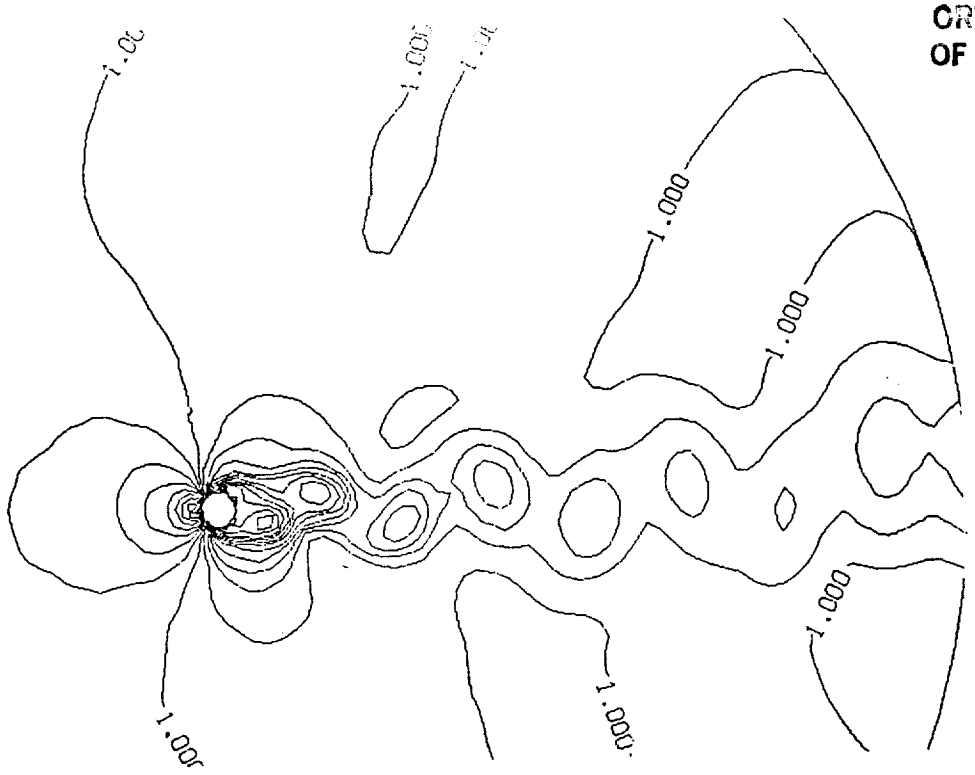

Figure 5.1a: Density contour plot of the spectral scheme SP1 at Time = 803.255 .

Figure 5.1b: Temperature contour plot of the spectral scheme SP1 at Time = 803.255 .

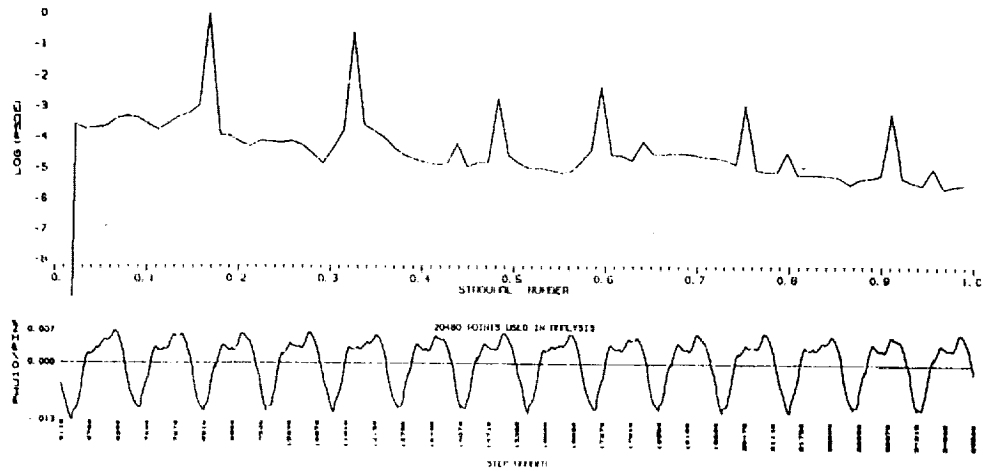

Figure 5.2a: Pressure time series and power density spectrum of the spectral scheme SP1 at the point located $10D$ behind the cylinder and $1D$ above the wake centerline.

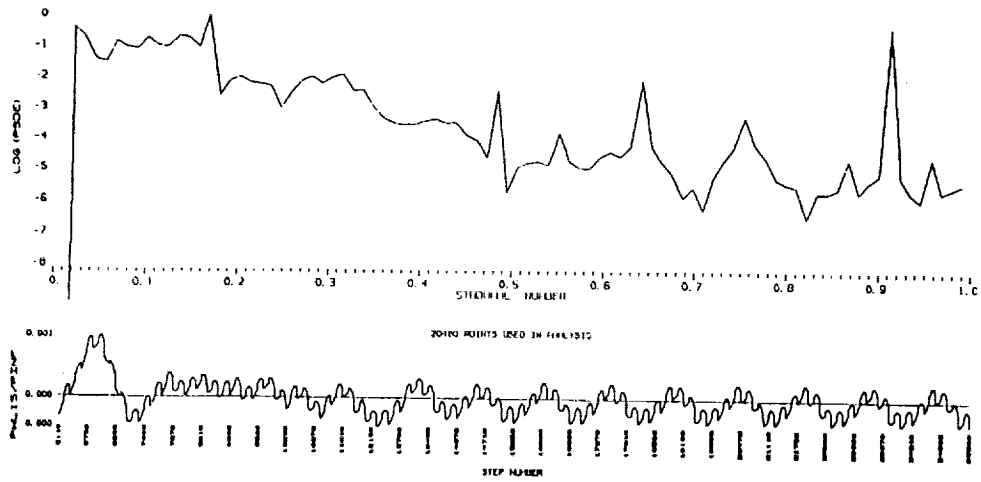

Figure 5.2b: Pressure time series and power density spectrum of the spectral scheme SP1 at the point located $10D$ away from the cylinder center and 180 degrees around the cylinder in the inflow region.

NASA
National Aeronautics and Space Administration

Report Documentation Page

1. Report No.	2. Government Accession No.	3. Recipient's Catalog No.
NASA CR-182030 ICASE Report No. 90-29		

4. Title and Subtitle

SPECTRAL SIMULATION OF UNSTEADY COMPRESSIBLE FLOW PAST A CIRCULAR CYLINDER

5. Report Date

April 1990

6. Performing Organization Code

7. Author(s)

Wai-Sun Don
David Gottlieb

8. Performing Organization Report No.

90-29

10. Work Unit No.

505-90-21-01

9. Performing Organization Name and Address

Institute for Computer Applications in Science and Engineering
Mail Stop 132C, NASA Langley Research Center
Hampton, VA 23665-5225

11. Contract or Grant No.

NAS1-18107, NAS1-18605

13. Type of Report and Period Covered

Contractor Report

12. Sponsoring Agency Name and Address

National Aeronautics and Space Administration
Langley Research Center
Hampton, VA 23665-5225

14. Sponsoring Agency Code

15. Supplementary Notes

Langley Technical Monitor:
Richard W. Barnwell

To appear in the Proceedings of the ICOSAHOM 1989

Final Report

16. Abstract

An unsteady compressible viscous wake flow past a circular cylinder has been successfully simulated using spectral methods. A new approach in using Chebyshev collocation method for periodic problem is introduced. We have further proved that the eigenvalues associated with the differentiation matrix are purely imaginary, reflecting the periodicity of the problem. It had been shown that the solution of a model problem has exponential growth in time if "improper" boundary conditions procedure is used. A characteristic boundary condition, which is based on the characteristics of the Euler equations of gas dynamics, has derived for the spectral code. Teh primary vortex shedding frequency computed agress well with the results in the literature for Mach = 0.4, Re = 80. No secondary frequency is observed in the power spectrum analysis of the pressure data.

17. Key Words (Suggested by Author(s))	18. Distribution Statement
spectral methods, flow past cylinders, boundary conditions for hyperbolic equations	02 - Aerodynamics 64 - Numerical Analysis Unclassified - Unlimited

19. Security Classif. (of this report)	20. Security Classif. (of this page)	21. No. of pages	22. Price
Unclassified	Unclassified	24	A03